EJNMMI Research

ORIGINAL RESEARCH

Open Access

P2X$_7$-receptor binding in new-onset and secondary progressive MS – a [^{11}C] SMW139 PET study

Jussi Lehto[1,2,3*], Richard Aarnio[1], Jouni Tuisku[1], Marcus Sucksdorff[1,2,4], Esa Mikko Koivumäki[1], Marjo Nylund[1,2,3,4], Semi Helin[1], Johan Rajander[1,5], Jonathan Danon[6], Jayson Gilchrist[6], Michael Kassiou[6], Vesa Oikonen[1] and Laura Airas[1,2,3,4]

Abstract

Background PET imaging of activated microglia has improved our understanding of the pathology behind disability progression in MS, and pro-inflammatory microglia at 'smoldering' lesion rims have been implicated as drivers of disability progression. The P2X$_7$R is upregulated in the cellular membranes of activated microglia. A single-tissue dual-input model was applied to quantify P2X$_7$R binding in the normal appearing white matter, perilesional areas and thalamus among progressive MS patients, healthy controls and newly diagnosed relapsing MS patients.

Results Overall, tracer uptake in the MS brain was not significantly higher compared to HCs. In the 3 mm perilesional rim of all T1 lesions, tracer binding was higher among relapsing patients compared to progressive patients. Tracer binding was higher in males compared to females. Disease duration correlated with tracer binding in the normal appearing white matter. Age correlated negatively with tracer binding in the perilesional rims.

Conclusions Even as binding estimates obtained with the dual-input model were consistent with the expected distribution of P2X$_7$Rs in the MS brain, the small free fraction of the parent tracer may limit its accuracy and applicability, and binding estimates between subjects were highly variable. Conclusive evidence for the applicability of [^{11}C]SMW139 to detect MS-related diffuse smoldering inflammation was not obtained.

Keywords Multiple sclerosis, Microglia, PET, Kinetic modelling

*Correspondence:
Jussi Lehto
juleht@utu.fi
[1]Turku PET Centre, Turku, Finland
[2]Neurocenter, Turku University Hospital, Turku, Finland
[3]InFLAMES Research Flagship, University of Turku, Turku, Finland
[4]Clinical Neurosciences, University of Turku, Turku, Finland
[5]Åbo Akademi University, Turku, Finland
[6]School of Chemistry, The University of Sydney, Sydney, Australia

Background

During the last two decades, extensive use of 18-kDa translocator protein positron emission tomography (TSPO-PET) [1] in in vivo imaging of activated microglia [2] has improved our understanding of the pathology behind disability progression [3–5] and treatment outcomes [6–9] in multiple sclerosis (MS). The translational applicability of this method is somewhat limited by its inability to distinctly differentiate between pro-inflammatory and anti-inflammatory phenotypes of activated microglia [10]. Activation of pro-inflammatory microglia at 'smoldering' lesion rims has been implicated as a driver of disability progression in MS [11, 12].

The adenosine triphosphate -gated cation channel receptor ($P2X_7R$) is upregulated in the cellular membranes of activated microglia [13] and has been identified as a potential therapeutic [14] and imaging target [10] in neurodegenerative disease, which offers improved specificity towards microglia that are in the pro-inflammatory end of the phenotype spectrum. The $P2X_7R$ activates the inflammasome, and results in pro-inflammatory interleukin release and proliferation of activated microglia [13, 15]. Compared to non-stimulated and homeostatic microglia in vitro, microglia polarized into an inflammatory phenotype over-express the $P2X_7R$ 5-folds, whereas a mere 1.5-fold difference is seen in TSPO expression [10]. In rodents, bacterial lipopolysaccharide –induced neuroinflammation leads to significant brain uptake of $P2X_7R$-specific radiotracers [16, 17], and uptake is also high at the peak of the MS disease model experimental autoimmune encephalitis (EAE) [18]. While also found on neurons and other glial cells, $P2X\times_7R$ signaling is primarily associated with activated inflammatory microglia [14, 19].

SMW139 is a potent antagonist (Ki 32 nM) of the $P2X_7R$ [20]. A mouse biodistribution study with radiolabeled [^{11}C]SMW139 demonstrated rapid brain uptake and clearance via liver metabolism: brain standardized uptake values decreased approximately 80–90% fom 5 min to 45 min post injection (p.i.) [21]. According to Akaike information criterion (AIC) [22], a reversible 90-minute two-tissue compartment model (2TCM) with a blood volume parameter provided the best fit for [^{11}C]SMW139 kinetics in a first in man study. Increased volumes of distribution (V_T) were observed among MS patients compared to healthy controls throughout the cerebral white matter, cortical grey matter (cGM) and deep gray matter (dGM) including the thalamus [23].

However, the specific tissue compartment of [^{11}C]SMW139 is small [23], and rapid metabolism results in a significant fraction of activity from brain-penetrant radiometabolites [21, 24, 25]. It is debatable whether a single-input 2TCM improves the fit by correcting for unspecific radiometabolite activity, rather than providing an accurate estimate of specific parent tracer binding. To address this, Aarnio et al. [24] utilized a rapid analysis method, which combines thin-layer chromatography with digital autoradiography for the parent fraction analysis. It was concluded that a dual-input (DI) function improves the quantification of specific [^{11}C]SMW139 binding [25].

In the current study we applied a single tissue compartment dual-input (1TDI) model to obtain estimates for the ratios of parent tracer rate constants between the blood compartment and the tissue compartment (k1p/k2p; V_{TDI} i.e. V_{T_parent}). We also aimed to further validate [^{11}C]SMW139 for MS studies by imaging progressive MS (PMS) patients with longer disease duration and no recent disease activity, and compared tracer binding in the normal appearing white matter (NAWM), perilesional areas and the thalamus to healthy controls, and to newly diagnosed relapsing MS (RMS). We also tested whether tracer uptake is increased around MS lesions by comparing perilesional V_T to lesional and NAWM V_T.

Methods

Subjects and procedures

The study was performed at the Turku PET Centre. Recruitment took place at the Turku University Hospital Neurocenter between Feb 2019 and Jun 2022. Inclusion criteria for all MS patients included a confirmed diagnosis according to the 2017 McDonald criteria and a written informed consent. Additional requirements were at least one Gd+lesion of at least 0.5 cm in diameter, and a clinical diagnosis of secondary progression for the RMS and PMS cohorts, respectively. Key exclusion criteria included pregnancy, claustrophobia, and other significant central nervous system pathology besides MS. All MS patients underwent baseline neurological assessments, magnetic resonance imaging (MRI) and [^{11}C]SMW139 PET. Age matched healthy control subjects (HCs) were imaged for comparison. The study protocol was approved by the Ethics Committee of the Hospital District of Southwest Finland. The study was conducted according to the principles of the Declaration of Helsinki.

[^{11}C]SMW139 production and PET

Irradiations were performed with a TR-19 (ACSI, Richmond, Canada) cyclotron to produce the carbon-11 radioisotope according to previously described procedures [8]. The complete synthesis procedure of [^{11}C]SMW139 at the Radiopharmaceutical Chemistry Laboratory of Turku PET Centre is described in the supplementary material of Aarnio et al. 2022 [24].

A ninety-minute dynamic PET scan was acquired for each subject with a high-resolution research tomograph (HRRT; Siemens Medical Solutions, Knoxville, TN, USA). The mean (SD) injected specific activity and mass

of [^{11}C]SMW139 were 95 (88) MBq/nmol and 2.7 (1.7) µg, respectively. The mean (SD) injected dose of radioactivity was 402 (12.2) MBq, 404 (13.5) MBq and 404 (10.7) MBq in the RMS, PMS and HC groups, respectively. List mode data was histogrammed into 21 timeframes (3×5s, 3×10s, 4×60s, 2×150s, 2×300s, 7×600s) and reconstructed using an OP-OSEM3D algorithm with 16 subsets and 10 iterations and with point spread function modelling [26] to reduce the partial volume effect. Reconstructed images were post-processed with a 2.5 mm FWHM (full width at half maximum) Gaussian filter.

Arterial blood sampling and PET modelling

A hematocrit sample was drawn within 1 h before PET imaging. An automated blood pump (ABSS, Allogg AB, Mariefred, Sweden) running at 60 rpm (6 mL/min) was used to obtain a continuous arterial blood time activity curve (TAC) from 0 to 5 min p.i., and manual arterial blood sampling ensued at 5, 10, 20, 40, 60, 75 and 90 min p.i. Arterial plasma activity were then converted to whole blood with individual plasma-to-blood ratio curves. Next, input curves for PET modelling were estimated by fitting the parent fraction with a monoexponential function $f(x) = (A\text{-}B)e^{-Cx} + B$, where A=1, B>=0, C>0, and multiplied with the arterial plasma data to obtain metabolite corrected arterial input TACs. The resulting curves were subtracted from the uncorrected plasma input curves to obtain the TACs corresponding to the radioactive metabolites in plasma. The differences in appearance times of radioactivity between PET and plasma, whole blood and metabolite TACs were corrected by first estimating the delay of the arterial plasma input TAC, which produced the best fit of two-tissue compartment model to whole brain TAC, and then shifting all other input TACs accordingly. Cerebral blood volume was fixed to 5% in all tested models.

The 1TDI model was fitted with five parameters (V_B, K_{1P}, K_{2P}, K_{1M}, K_{2M}; P=parent, M=metabolite). The distribution volume of [^{11}C]SMW139 was estimated with the ratio of rate constants of the intact parent tracer between the plasma compartment and the combined tissue compartment; K_{1P}/K_{2P} (V_{TDI}). Additionally, tracer binding was quantified with the total volume of distribution V_{T2T} of a reversible 2TCM, where the model was fitted with five parameters (V_B, K_1, K_2, K_3, K_4) and where $V_{T2T} = K_1/K_2(1+K_3/K_4)$. The modelling was carried out with in house software (fitk2di and fitk4; http://www.turkupetcentre.net/programs/doc/).

Parent fraction and plasma protein binding of the parent tracer and its radiometabolites

Arterial blood samples were drawn at 0, 5, 10, 20, 40, 60 and 90 min p.i. and the plasma was separated by centrifugation (4 °C, 2118 g, 5 min). The plasma proteins were precipitated by adding 700 µL of acetonitrile to 500 µL of plasma, vortexing and centrifuging (3370 g, 3 min). The protein free supernatant was analyzed with high-performance liquid chromatography (HPLC) using a method described in the supplementary material of Brumberg et al. [25] to obtain fractions of intact [^{11}C]SMW139 and its radioactive metabolites for correcting the plasma TAC. A radioactive standard was prepared by spiking the time point 0 plasma supernatant with [^{11}C]SMW139 in order to analyze the correct peak of the chromatograms to correspond to the parent.

Parent and radiometabolite binding to plasma proteins was analyzed for a subset of subjects from blood samples drawn prior to [^{11}C]SMW139 injection and from 20 min p.i. From the time point 0 plasma drawn for in vitro protein binding analysis, 1 mL was frozen for later duplicate analysis. The in vitro plasma and in vivo 20 min parent fraction analysis plasma samples were used to analyze parent and radiometabolite plasma protein binding with separate ultrafiltration membrane corrections.

MRI and PET image processing and analysis

A 3T MRI (Philips Ingenia/Philips Ingenuity, Best, The Netherlands) was acquired for all study participants with T1, T2, FLAIR, 3DT1, and gadolinium-enhanced T1. The dynamic PET images were smoothed, realigned, and co-registered using statistical parametric mapping (SPM12; Wellcome Trust Center for Neuroimaging, London, UK) according to a previously described procedure [6]. The images were resliced to match the 1-mm^3 voxel size of the MRI images.

The Lesion Segmentation Toolbox (LST) [27] was used in SPM to create FLAIR masks, which were manually edited to correspond to chronic T1 lesions to create T1 masks following a previously described procedure [8]. Perilesional masks were created by dilating the lesion mask by 3 mm, and then subtracting the core image from the dilated image. Separate masks were created for the Gd+lesions. NAWM masks were created for each subject by subtracting edited FLAIR lesion masks from segmented white matter. Finally, T1 images were filled with the T1 masks by employing the lesion filling tool of LST in SPM. The filled T1 image was used to segment whole-brain volume (BV) and volumes of different brain areas with FreeSurfer (https://surfer.nmr.mgh.harvard.edu/) for PET assessments.

Statistical analysis

The statistical analysis was performed with SPSS 28.0 (IBM Corp., Armonk, NY, USA). Figures were created with Prism 10.1.2 (GraphPad software Inc. La Jolla, CA, USA). Group level means of V_T estimates across different brain areas were compared between MS patients and

HCs, and between PMS and RMS with Student's t-test. Among MS patients, Group level means of V_T estimates were compared between the T1 lesion masks, the 3 mm perilesional rim masks, and the NAWM masks with paired t-tests. Normality of the data was confirmed with the Shapiro-Wilk test. Linear correlations between V_T estimates, lesion volume, BV, thalamus volume, and demographic variables were measured with the Pearson correlation coefficient. The effects of disease duration and BV on V_{TDI} were estimated with multiple linear regression. All tests were two-tailed, and the alpha was set to 0.05 for all analyses with no correction for multiple comparisons.

Results

Study subject demographics and other baseline characteristics

26 subjects underwent the study procedures and the final analyzed cohorts consisted of 15 MS patients ($n=6$ for RMS, $n=9$ for PMS) and 9 HCs. 2 subjects (1 PMS and 1 HC) were excluded from the analysis due to technical issues during the PET visits. All RMS patients were enrolled < 0.5 years (mean 0.12 years, SD 0.06) from diagnosis and PET imaged with [^{11}C]SMW139 approximately 4 months thereafter. PMS patients were imaged > 10 years (mean 16.9 years, SD 4.3) from diagnosis immediately after inclusion. Compared to patients with MS, the HCs were of comparable age [mean (SD) 47,5 (10.1) vs. 49.6 (14.5) years, $p=0.479$, respectively]. Compared to the RMS patients, the PMS cohort had a significantly higher EDSS (median 2.0 vs. 6.0, mean 2.5 vs. 5.1, $p=0.005$, respectively), and the two patient cohorts were of comparable age [mean (SD) 45.0 (11.7) vs. 49.2 (9.3) years, $p=0.712$, respectively]. The male to female (M/F) ratio was unequal between all cohorts but comparable between all MS and HCs: 6/3 (33% F), 9/6 (40% F), 4/5 (56% F) and 5/1 (17% F) for HCs, MS, PMS and RMS, respectively. At the time of PET imaging, two patients in the RMS cohort had started treatment with i.v. natalizumab, 1 patient had received a single dose of i.v ocrelizumab, and 3 patients had received a single i.v. dose of rituximab. Three PMS patients were treated with rituximab, one with natalizumab, and one with fingolimod. MS lesion loads and other imaging characteristics are displayed in Table 1.

Parent fraction and protein binding of [^{11}C]SMW139

The plasma parent fraction decreased steadily down to approximately 45% over the course of the 90 min sampling time. The mean parent fraction in the PMS group was indicative of slightly faster metabolism, while metabolism of [^{11}C]SMW139 was non-significantly slower among the RMS and HC groups (Fig. 1).

The plasma protein binding analysis of frozen and fresh plasma samples yielded similar results. The mean (SD) parent free fraction (free parent over all parent in plasma, $f_{P/P}$) of [^{11}C]SMW139 was 0.013 (0.004) and 0.013 (0.002) ($n=11$ for both) for fresh and frozen samples, respectively, and 0.010 (0.004) ($n=9$) for the in vivo 20 min sample. The mean (SD) fraction of free radiometabolites over all radiometabolites was 0.425 (0.132) and the fraction of free radiometabolites over all free radioactivity in plasma was 0.88 (0.06) at 20 min. The mean $f_{P/P}$ was

Table 1 MRI variables and [^{11}C]SMW139 V_{TDI} (0–60 min)

	n	Min.	Max.	Mean	SD	*p*
Brain Volume (cm^3) HC	9	939.20	1267.21	1148.24	109.16	0.665*
Brain Volume (cm^3) RMS	6	1069.40	1231.09	1172.81	61.34	0.276**
Brain Volume (cm^3) PMS	9	814.63	1347.18	1055.53	173.10	
T1 lesion volume (cm^3) RMS	6	2.12	48.17	17.21	18.45	0.940**
T1 lesion volume (cm^3) PMS	9	2.62	44.14	16.60	12.57	
Number of Gd + lesions RMS	6	1	20	8.33	7.97	NA
SMW V_{TDI} T1 lesions RMS	6	0.09	0.14	0.11	0.02	0.194**
SMW V_{TDI} T1 lesions PMS	9	0.02	0.12	0.09	0.03	
SMW V_{TDI} 3 mm rim RMS	6	0.11	0.15	0.12	0.02	0.113**
SMW V_{TDI} 3 mm rim PMS	9	0.03	0.14	0.10	0.03	
SMW V_{TDI} Thalamus HC	9	0.03	0.32	0.13	0.09	0.723*
SMW V_{TDI} Thalamus RMS	6	0.10	0.19	0.14	0.03	0.071**
SMW V_{TDI} Thalamus PMS	9	0.04	0.16	0.11	0.04	
SMW V_{TDI} NAWM HC	9	0.04	0.16	0.11	0.04	0.962*
SMW V_{TDI} NAWM RMS	6	0.09	0.14	0.12	0.02	0.121**
SMW V_{TDI} NAWM PMS	9	0.04	0.14	0.10	0.03	

*For the comparison all MS vs. HC

**For the comparison RMS vs. PMS

V_{TDI} = dual-input distribution volume of parent tracer (K_{1P}/K_{2P}). 3 mm rim = T1 perilesional 3 mm rim. NAWM = Normal appearing white matter. HC = Healthy control. RMS = Relapsing MS. PMS = Progressive MS

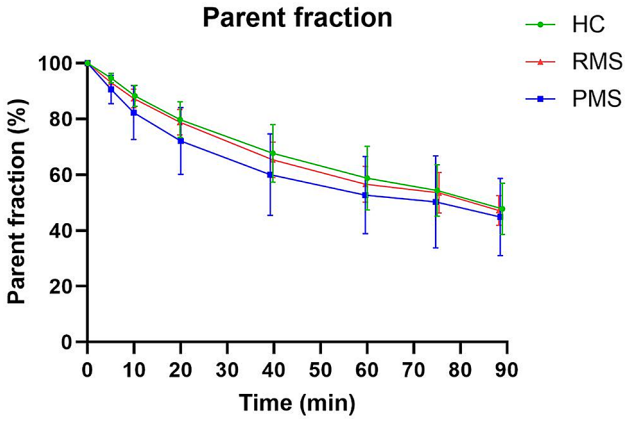

Fig. 1 The mean percentages of unchanged [^{11}C] SMW139 of the total radioactivity in the plasma samples (parent fraction) of the healthy controls (HC), relapsing MS (RMS) and progressive MS (PMS)

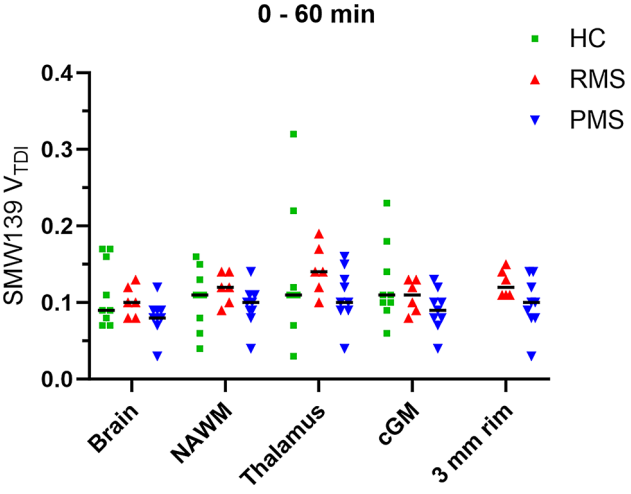

Fig. 2 [11 C]SWM139 V_{TDI} (0–60 min) in the normal appearing white matter (NAWM), thalamus, cortical gray matter (cGM) and T1 perilesional 3 mm rim (3 mm rim) among healthy controls (HC), relapsing MS (RMS) and progressive MS (PMS)

0.0138 (n=3), 0.0096 (n=5) and 0.0093 (n=3) for HCs, PMS and RMS, respectively.

PET modelling

According to visual inspection (Supplement 1), AIC and logarithm of mean residual sum of squares (log (1/n) (model – data)^2, where n=no. data points) (Supplement 2), both tested models fitted the data well. Coefficients of variation (CoV) of V_T estimates were substantially higher with the 2TCM (Supplement 2). Compared to HCs, the overall performance of 1TDI was better among MS patients, and 0–40 min and 0–60 min performed similarly according to AIC (Supplement 3). Finally, 0–60 min data was chosen for the primary analyses based on marginally lower CoV compared to 0–40 min and 0–90 min (Supplement 2–3). Additional exploratory analyses were performed with 0–40 min and 0–90 min data for

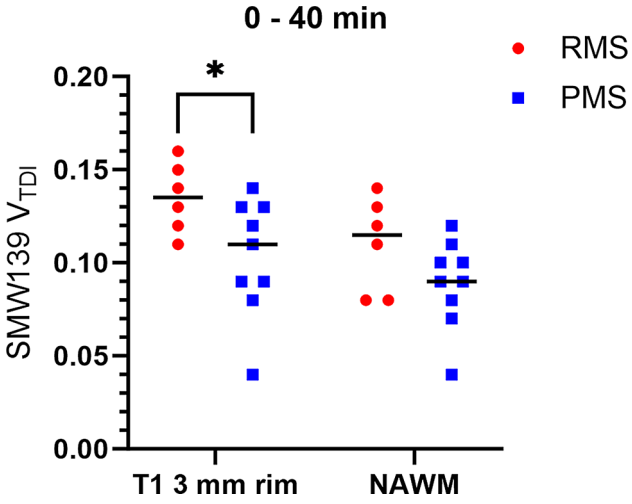

Fig. 3 T1 perilesional 3 mm rim and normal appearing white matter (NAWM) among relapsing MS (RMS) and progressive MS (PMS). *p = 0.049

the 1TDI and 2TCM models, respectively. V_T estimates from thalamus (R=0.800, p<0.001) and cGM (R=0.630, p<0.001) correlated significantly between the models (0–60 min 1TDI and 0–90 min 2TCM), while estimates from NAWM (R=0.158, p=0.461) and lesional or perilesional (R=-0.04, p=0.888) white matter did not.

[^{11}C]SMW139 binding in RMS and PMS patients compared to healthy control subjects

Compared to healthy controls, whole-brain, NAWM, thalamic and cGM uptake of [^{11}C]SMW139 was similar in MS patients (n=15) at group level. After explorative correction for group level mean $f_{P/P}$ (V_{TDI} / $f_{P/P}$), mean (SD) NAWM V_{TDI} was significantly higher among all MS compared to HCs [11.15 (3.09) vs. 7.69 (2.80), p=0.012, respectively].

V_{TDI} estimates were somewhat higher in the RMS cohort compared to PMS and HCs, but the differences were not statistically significant (Table 1; Fig. 2). In the 3 mm perilesional rim of all T1 lesions, the mean (SD) V_{TDI} was 0.123 (0.02) vs. 0.097 (0.03) (p=0.113) in the RMS and PMS cohorts, respectively. Exploratory analysis with 0–40 min data revealed a significant difference between the two groups [Fig. 3.133 (0.02) vs. 0.101 (0.03), p=0.049, respectively]. The 2TCM yielded no significant differences between the groups, when all MS was compared to HCs (Supplement 4), or when RMS was compared to PMS (Supplement 5).

Exploratory analysis of [^{11}C]SMW139 binding in MS lesions compared with NAWM and the perilesional areas

Compared to MS lesion core areas, V_{TDI} estimates were significantly higher in the NAWM and perilesional 3 mm rims among all MS patients (Table 2; Fig. 4). Analyzed separately, perilesional tracer uptake was significantly

Table 2 Lesional, perilesional and NAWM [^{11}C]SMW139 V_{TDI}

Comparison	Mean	SD	*p*
3 mm rim - T1 lesions MS	0.0123	0.0140	**0.004**
3 mm rim - NAWM MS	0.0017	0.0124	0.611
NAWM MS - T1 lesions MS	0.0106	0.0176	**0.034**
3 mm rim - T1 lesions PMS	0.0097	0.0144	0.078
3 mm rim - NAWM PMS	0.0007	0.0136	0.879
NAWM PMS - T1 lesions PMS	0.0090	0.0178	0.170
3 mm rim - T1 lesions RMS	0.0162	0.0138	**0.034**
3 mm rim - NAWM RMS	0.0031	0.0114	0.536
NAWM RMS - T1 lesions RMS	0.0131	0.0185	0.143
Gd + T1 lesions - T1 lesions RMS	0.0067	0.0138	0.403
Gd + 3 mm rim – 3 mm rim RMS	0.0164	0.0510	0.623

3 mm rim = T1 perilesional 3 mm rim, NAWM = Normal appearing white matter RMS = Relapsing MS. PMS = Progressive MS

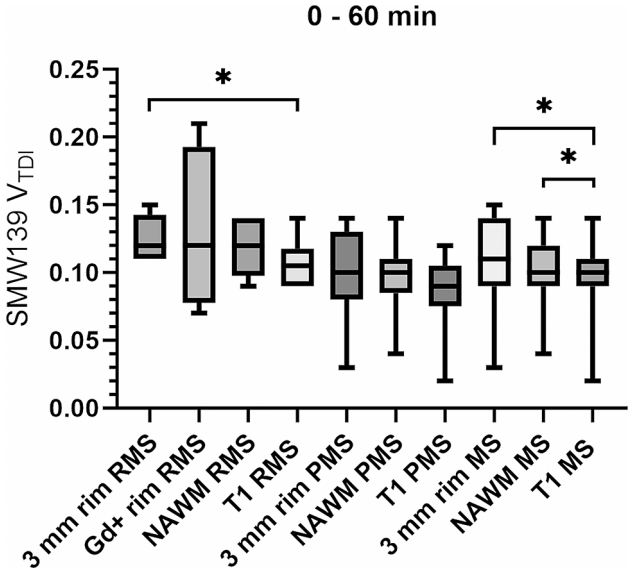

Fig. 4 [11 C]SWM139 V_{TDI} in the 3 mm perilesional rims, normal appearing white matter (NAWM) and T1 lesions among relapsing MS (RMS), progressive MS (PMS) and all MS. ***p* < 0.05** (Table 2 for pairwise comparisons)

higher compared to lesions among RMS patients, but not among PMS patients. V_{TDI} estimates within the Gd+lesions and in the 3 mm rim around Gd+lesions were not significantly higher compared to all RMS T1 lesions and the perilesional 3 mm area in general, respectively (Table 2). Lesional V_{T2T} estimates were significantly higher compared to the NAWM and the perilesional area among all MS patients. (Supplement 6).

Exploratory analysis of [^{11}C]SMW139 binding in relation to demographic characteristics and MRI variables

Age correlated negatively with V_{TDI} in the 3 mm perilesional area among all MS patients (R= -0.558, p=0.031; Fig. 5B), and non-significantly with NAWM V_{TDI} (R= -0.465, p=0.081), but no correlation with NAWM V_{TDI} was seen among all subjects (n=24, R=0.024, p=0.91). Among all MS patients or among RMS or PMS, V_{TDI} estimates did not correlate with EDSS (results not shown). Among PMS patients, time from diagnosis correlated with NAWM V_{TDI} (Fig. 5). Of note, BV or age did not correlate with disease duration among PMS patients (R= -0.259, p=0.501 and R= -0.350, p=0.365, respectively). Among all subjects, V_{TDI} estimates in the NAWM correlated with BV, and the same was true for the 3 mm perilesional rim among all MS (Fig. 5).

Among PMS with NAWM V_{TDI} as the dependent variable, both disease duration (β=0.561, t=2.603, p=0.041) and BV (β=0.547, t=2.536, p=0.044) added significantly to the prediction (R^2=0.855, F(2,6)=8.166, p=0.019). V_{TDI} in the perilesional area or NAWM did not correlate with overall T1 lesion volume (results not shown). No significant correlations with V_{T2T} estimates and demographic variables or brain or lesion volume were found with the 2TCM model. V_{TDI} estimates and BV were significantly higher among male subjects compared to females across all examined brain areas. The two groups were of similar age and EDSS, and lesion volumes were comparable, but the time from diagnosis among female subjects was somewhat longer (p>0.05, Supplement 7). The correlation of NAWM V_{TDI} with BV was abolished (R=0.076, p=0.791), when all male subjects (n=15) were analyzed separately.

Discussion

Even though uptake in the 3 mm perilesional rims of T1 lesions suggested in vivo sensitivity towards activated microglia in MS, tracer uptake in this cohort of MS patients was not significantly higher compared to HCs. Exploratory analyses indicated increased tracer binding in the NAWM among subjects with longer disease duration, which is consistent with previous MS imaging studies indicating diffuse activation of microglia in the NAWM as MS progresses [4, 12], but this finding is to be interpreted with caution. Despite high affinity of [^{11}C] SMW139 for inflammatory microglia [10], the wide range of $P2X_7R$-expression across different neural and cellular targets [28] may have influenced the highly variable binding estimates, and reduced accuracy with regards to inflammatory microglia.

Hagens and colleagues reported somewhat improved single-input 2TCM fits with longer p.i. time and, due to unreliable estimation of the disassociation rate (k4) in smaller regions of interest (ROIs), by binding k4 to the whole-brain value [23]. Even as all kinetic parameters were fitted with the 2TCM in the present study, higher V_{T2T} inside MS lesions compared to the surrounding white matter (Supplement 6) was consistent with previously published findings [23], where a discrepancy with lesional binding potential estimates was also observed. In the present study, thalamic and cGM V_T estimates correlated moderately and strongly between 1TDI and 2TCM,

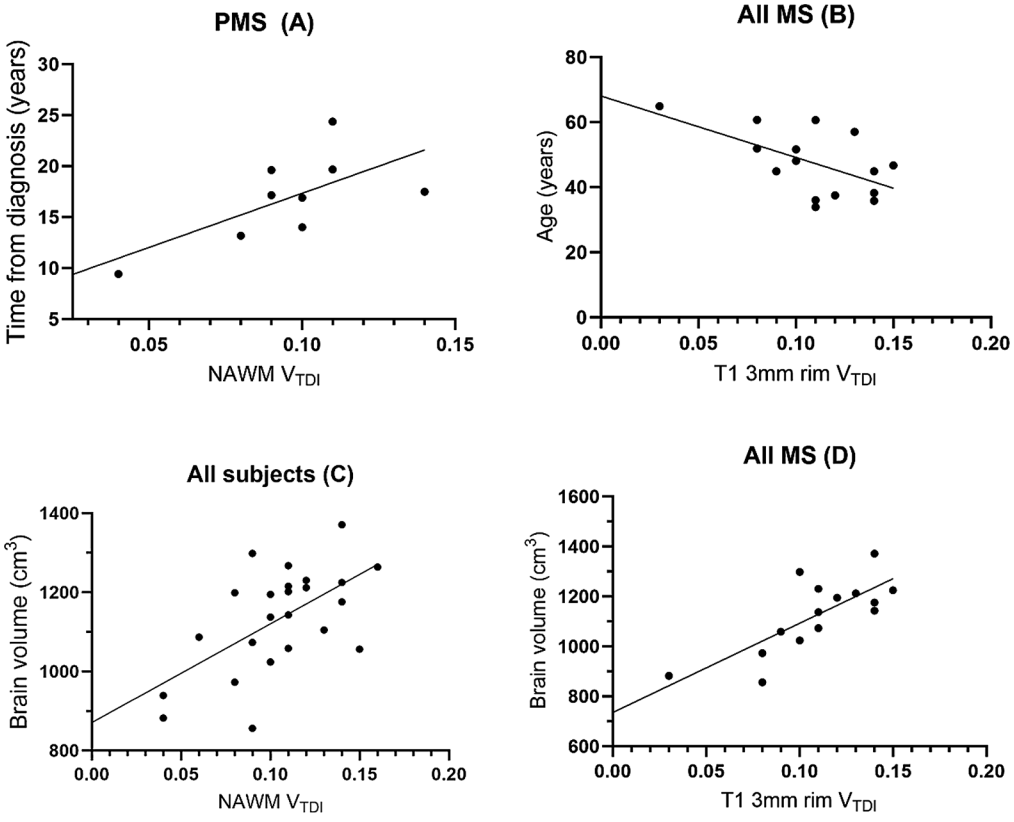

Fig. 5 V_{TDI} in the normal appearing white matter (NAWM) among progressive MS (PMS) correlated with disease duration (A; $R = 0.666$, $p = 0.05$). V_{TDI} in the T1 perilesional 3 mm rim among all MS correlated with age (B; $R = -0.558$, $p = 0.031$). V_{TDI} in the NAWM among all subjects correlated with brain volume (C; $R = 0.577$, $p = 0.003$). V_{TDI} in the T1 perilesional 3 mm rim among all MS correlated with brain volume (D; $R = 0.734$, $p = 0.002$)

respectively, while WM estimates did not. Considering the above, it is deemed likely that two-compartment models improve AIC with [^{11}C]SMW139 by fitting radiometabolite build-up between the tissue compartments, and this effect is accentuated with longer fits. A strong correlation between the 1TDI and 2TCM was seen in the cGM, an area with a relatively scarce distribution of activated microglia in MS [29].

In addition, Brumberg and colleagues reported markedly superior 2TDI AIC only in the cGM, whereas the 1TDI was associated with robust fits across all examined regions, and with somewhat lower %SE [25]. A 2TDI model does not reliably fit in all cases and smaller regions of interest with [^{11}C]SMW139, while the 1TDI could be more sensitive to inaccuracies in plasma input data. The locus of interest [7, 30–32] in MS brain imaging is primarily in the NAWM, where the 1TDI performed significantly better in the present study compared to previous GM fits [25] according to AIC, and in small perilesional WM regions, where estimates may also be affected by the partial volume effect. Based on the above, 1TDI was chosen for the primary analysis. In addition to CoV and AIC, the 0–60 min fit was preferred based on the theoretically reduced effect of radioactive metabolites, while it was also assumed that fits significantly below 60 min would describe the data inadequately. Together with rapid tracer metabolism, the 20-min half-life of carbon-11 reduces the reliability estimates beyond 60 min p.i. even further.

Beyond pharmacokinetic considerations, a viable PET model is expected to produce estimates of target engagement that are in line with the known distribution of the tracer's cognate receptors. In MS, microglia-associated TSPO expression is concentrated to active lesions and chronic lesion rims, and to a lesser extent chronic lesion centers and the NAWM, while inactive lesions and grey matter lesions are relatively devoid of microglia. HLADR+inflammatory microglia are most abundant at chronic lesion rims [29]. Similarly, $P2X_7R$-expression is more prominent in acute active lesions and chronic active lesion rims [10]. Compared to chronic and chronic active lesions, acute active MS lesions represent a small fraction of overall lesion count [33, 34]. The fraction of early active lesions declines rapidly, and has been estimated to represent < 5% of all lesios at 5–10 years after disease onset [33].

Thus it was postulated that at group level, most specific binding of [^{11}C]SMW139 in the WM of MS patients would take place in the immediate area around T1

lesions, and that lesional binding would decline after the initial phase of the disease. In the current study, perilesional binding was significantly higher than lesional binding, but not significantly higher than NAWM binding. In the newly diagnosed cohort of RMS, perilesional tracer binding was increased compared to PMS patients, although it is acknowledged that the groups were not sex-matched. Lesions that Gd-enhanced approximately 4 months prior to PET imaging did not exhibit significantly higher tracer uptake, which indicates that disruption of the blood brain barrier did not significantly affect perilesional binding estimates among RMS.

The free fraction of [^{11}C]SMW139 was low, while radiometabolites contributed significantly to overall radioactivity passing through the blood brain barrier. 88% of the free radioactivity was due to circulating radiometabolites at 20 min. Estimates obtained by using protein binding to correct V_{TP} are susceptible to minor errors in $f_{P/P}$ analysis, and thus correcting for the group level mean of the free parent was explored. This resulted in a significantly higher mean free parent V_T among MS patients compared to HCs, but incomplete protein binding data precludes conclusions on group level differences based on this sub-analysis. This approach should be considered in subsequent studies with [^{11}C]SMW139.

[^{11}C]SMW139 uptake was significantly increased in male subjects compared to females, and the strong correlation with BV was completely abolished when male subjects were analyzed separately. A similar sex disparity in tracer uptake has been observed with the microglial TSPO tracer [^{11}C]PK11195 [35]. While it is acknowledged that genetic polymorphism of the $P2X_7R$ is considerable both between and within species [36], these findings are in agreement with sex-dependent purinergic receptor expression [37], and an inflammatory microglial transcriptome in male mice [38].

Interestingly, MS disease duration correlated with tracer uptake, and this correlation was not explained by age or sex, as disease duration was somewhat longer among females. Significant correlations with MS-related disability and NAWM uptake of [^{11}C]PK11195 have been reported previously [3, 4]. Also considering the higher uptake in RMS, lower tracer uptake in the perilesional rims among older subjects suggests that $P2X_7R$-signaling may be significant at the early stages of chronic active lesion formation. [^{11}C]SMW139 uptake peaks at the early stage of EAE [18].

Conclusions

No conclusive evidence for the applicability of [^{11}C]SMW139 to detect MS-related smoldering inflammation was obtained. Even though disease duration correlated with tracer binding in the NAWM, overall tracer uptake in the MS brain was not significantly higher compared to HCs. Age and sex are to be matched with a careful emphasis when studies with this tracer are conducted. Further information on the applicability of [^{11}C]SMW139 PET in MS could be obtained by correlating the current results with longitudinal clinical outcomes and progression-related biomarkers.

Abbreviations

TSPO	18-kDa translocator protein
$P2X_7R$	Adenosine triphosphate -gated cation channel receptor
AIC	Akaike information criterion
CoV	Coefficient of variation
cGM	Cortical grey matter
dGM	Deep gray matter
k4	Disassociation rate from the specific tissue compartment
V_{TDI}	Distribution volume of parent [11 C]SMW139
DI	Dual-input
EAE	Experimental autoimmune encephalitis
FWHM	Full width at half maximum
HC	Healthy control subject
HPLC	High-performance liquid chromatography
HRRT	High-resolution research tomograph
LST	Lesion segmentation toolbox
MRI	Magnetic resonance imaging
MS	Multiple sclerosis
NAWM	Normal appearing white matter
PET	Positron emission tomography
p.i.	Post injection
PMS	Progressive MS
ROI	Region of interest
RMS	Relapsing MS
1TDI	Single tissue compartment dual-input model
SD	Standard deviation
SPM	Statistical parametric mapping
TAC	Time activity curve
2TCM	Two-tissue compartment model
VT	Volume of distribution
BV	Whole-brain volume

Supplementary Information

The online version contains supplementary material available at https://doi.org/10.1186/s13550-024-01186-3.

Supplementary Material 1

Acknowledgements

Not applicable.

Author contributions

JL: Writing – original draft (lead), Writing - review and editing (lead), Visualization (lead), Investigation (equal), Formal analysis (equal). RA: Writing – original draft (supporting), Investigation (supporting), Writing - review and editing (supporting); Visualization (supporting). JT: Formal analysis (equal), Writing - review and editing (supporting). MS: Investigation (equal); Conceptualization (supporting). EMK: Investigation (equal). MN: Project management (lead); Funding acquisition (supporting), Investigation (supporting). SH: Resources (equal). JR: Resources (equal). JD: Investigation (supporting), Resources (supporting). JG: Investigation (supporting), Resources (supporting). MK: Supervision (supporting), Resources (supporting). VO: Formal analysis (supporting), Conceptualization (supporting). LA: Supervision (lead); Conceptualization (lead); Funding acquisition (lead); Writing – review and editing (supporting).

Funding

This work was supported by a grant from the National Multiple Sclerosis Society, The Jane and Aatos Erkko Foundation, The Research Council of Finland (decision number: 330902), the Sigrid Juselius Foundation, State research funding of the Turku University Hospital expert responsibility area,

Finnish Governmental Research Funding (VTR) for Turku University Hospital, and the InFLAMES Flagship Programme of The Research Council of Finland (decision number 337530).

Data availability

Any anonymized data used in the preparation of this article will be made available by the request of a qualified investigator.

Declarations

Ethics approval and consent to participate

The study was conducted according to the principles of the Declaration of Helsinki. All subjects were adults (> 18 years old), and provided written informed consent. The study was approved by the Ethics Committee of the Hospital District of Southwest Finland.

Consent for publication

Not applicable.

Conflict of interest

The authors have nothing to disclose.

Received: 13 June 2024 / Accepted: 20 November 2024
Published online: 05 December 2024

References

1. Chauveau F, Becker G, Boutin H. Have (R)-[11 C]PK11195 challengers fulfilled the promise? A scoping review of clinical TSPO PET studies. Eur J Nucl Med Mol Imaging. Springer Science and Business Media Deutschland GmbH; 2021. pp. 201–20.
2. Banati RB, Newcombe J, Gunn RN, Cagnin A, Turkheimer F, Heppner F et al. The peripheral benzodiazepine binding site in the brain in multiple sclerosis: Quantitative in vivo imaging of microglia as a measure of disease activity. Brain [Internet]. 2000;123:2321–37. https://doi.org/10.1093/brain/123.11.2321
3. Sucksdorff M, Matilainen M, Tuisku J, Polvinen E, Vuorimaa A, Rokka J et al. Brain TSPO-PET predicts later disease progression independent of relapses in multiple sclerosis. Brain [Internet]. 2020;143:3318–30. https://www.ncbi.nlm.nih.gov/pubmed/33006604
4. Rissanen E, Tuisku J, Vahlberg T, Sucksdorff M, Paavilainen T, Parkkola R et al. Microglial activation, white matter tract damage, and disability in MS. Neurol Neuroimmunol Neuroinflamm [Internet]. 2018;5:e443. https://www.ncbi.nlm.nih.gov/pubmed/29520366
5. Misin O, Matilainen M, Nylund M, Honkonen E, Rissanen E, Sucksdorff M et al. Innate Immune Cell–Related Pathology in the Thalamus Signals a Risk for Disability Progression in Multiple Sclerosis. Neurology - Neuroimmunology Neuroinflammation [Internet]. 2022;9:e1182. http://nn.neurology.org/content/9/4/e1182.abstract
6. Sucksdorff M, Tuisku J, Matilainen M, Vuorimaa A, Smith S, Keitilä J et al. Natalizumab treatment reduces microglial activation in the white matter of the MS brain. Neurol Neuroimmunol Neuroinflamm. 2019;6.
7. Lehto J, Sucksdorff M, Nylund M, Raitanen R, Matilainen M, Airas L. PET-measurable innate immune cell activation reduction in chronic active lesions in PPMS brain after rituximab treatment: a case report. J Neurol [Internet]. 2022 [cited 2023 Jan 24];1:1–4. https://link.springer.com/article/https://doi.org/10.1007/s00415-022-11539-4
8. Lehto J, Nylund M, Matilainen M, Sucksdorff M, Vuorimaa A, Rajander J et al. Longitudinal stability of progression-related microglial activity during teriflunomide treatment in patients with multiple sclerosis. Eur J Neurol [Internet]. 2023;n/a. https://doi.org/10.1111/ene.15834
9. Sucksdorff M, Rissanen E, Tuisku J, Nuutinen S, Paavilainen T, Rokka J, et al. Evaluation of the effect of fingolimod treatment on microglial activation using serial PET imaging in multiple sclerosis. J Nucl Med. 2017;58:1646–51.
10. Beaino W, Janssen B, Kooij G, van der Pol SMA, van Het Hof B, van Horssen J et al. Purinergic receptors P2Y12R and P2X7R: Potential targets for PET imaging of microglia phenotypes in multiple sclerosis. J Neuroinflammation [Internet]. 2017 [cited 2023 Feb 7];14:1–16. https://jneuroinflammation.biomedcentral.com/articles/https://doi.org/10.1186/s12974-017-1034-z
11. Giovannoni G, Popescu V, Wuerfel J, Hellwig K, Iacobeus E, Jensen MB et al. Smouldering multiple sclerosis: the 'real MS.' Ther. Adv Neurol Disord. 2022;15.
12. Nylund M, Sucksdorff M, Matilainen M, Polvinen E, Tuisku J, Airas L. Phenotyping of multiple sclerosis lesions according to innate immune cell activation using 18 kDa translocator protein-PET. Brain Commun. 2022;4.
13. Monif M, Burnstock G, Williams DA. Microglia: proliferation and activation driven by the P2X7 receptor. Int J Biochem Cell Biol [Internet]. 2010 [cited 2023 Jun 15];42:1753–6. https://pubmed.ncbi.nlm.nih.gov/20599520/
14. Bhattacharya A, Biber K. The microglial ATP-gated ion channel P2X7 as a CNS drug target. Glia [Internet]. 2016 [cited 2023 Jun 15];64:1772–87. https://pubmed.ncbi.nlm.nih.gov/27219534/
15. Clark AK, Staniland AA, Marchand F, Kaan TKY, McMahon SB, Malcangio M. P2X7-Dependent Release of Interleukin-1β and Nociception in the Spinal Cord following Lipopolysaccharide. The Journal of Neuroscience [Internet]. 2010 [cited 2023 Jun 15];30:573. /pmc/articles/PMC2880485/
16. Fantoni ER, Dal Ben D, Falzoni S, Di Virgilio F, Lovestone S, Gee A. Design, synthesis and evaluation in an LPS rodent model of neuroinflammation of a novel 18F-labelled PET tracer targeting P2X7. EJNMMI Res [Internet]. 2017 [cited 2023 Nov 24];7:1–12. https://link.springer.com/articles/https://doi.org/10.1186/s13550-017-0275-2
17. Territo PR, Meyer JA, Peters JS, Riley AA, McCarthy BP, Gao M et al. Characterization of 11 C-GSK1482160 for Targeting the P2X7 Receptor as a Biomarker for Neuroinflammation. J Nucl Med [Internet]. 2017 [cited 2023 Nov 24];58:458–65. https://pubmed.ncbi.nlm.nih.gov/27765863/
18. Beaino W, Janssen B, Kooijman E, Vos R, Schuit RC, O'Brien-Brown J et al. PET imaging of P2X7R in the experimental autoimmune encephalomyelitis model of multiple sclerosis using [11 C]SMW139. J Neuroinflammation [Internet]. 2020 [cited 2024 Feb 28];17:1–18. https://jneuroinflammation.biomedcentral.com/articles/https://doi.org/10.1186/s12974-020-01962-7
19. Burnstock G. P2X ion channel receptors and inflammation. Purinergic Signalling. 2016 12:1 [Internet]. 2016 [cited 2023 Jun 15];12:59–67. https://link.springer.com/article/10.1007/s11302-015-9493-0
20. Wilkinson SM, Barron ML, O'Brien-Brown J, Janssen B, Stokes L, Werry EL et al. Pharmacological Evaluation of Novel Bioisosteres of an Adamantanyl Benzamide P2X7 Receptor Antagonist. ACS Chem Neurosci [Internet]. 2017 [cited 2023 Jun 15];8:2374–80. https://pubs.acs.org/doi/full/10.1021/acschemneuro.7b00272
21. Janssen B, Vugts DJ, Wilkinson SM, Ory D, Chalon S, Hoozemans JJM et al. Identification of the allosteric P2X7 receptor antagonist [11 C]SMW139 as a PET tracer of microglial activation. Scientific Reports 2018 8:1 [Internet]. 2018 [cited 2023 Jun 15];8:1–10. https://www.nature.com/articles/s41598-018-24814-0
22. Akaike H. Information Theory and an Extension of Information the Maximum Theory Likelihood and an Principle Extension of the Maximum Likelihood Principle. Biogeochemistry [Internet]. 1998 [cited 2023 Jun 15];1998:199–213. https://link.springer.com/chapter/https://doi.org/10.1007/978-1-4612-1694-0_15
23. Hagens MHJ, Golla SSV, Janssen B, Vugts DJ, Beaino W, Windhorst AD, et al. The P2X7 receptor tracer [11 C]SMW139 as an in vivo marker of neuroinflammation in multiple sclerosis: a first-in man study. Eur J Nucl Med Mol Imaging. 2020;47:379–89.
24. Aarnio R, Alzghool OM, Wahlroos S, O'Brien-Brown J, Kassiou M, Solin O et al. Novel plasma protein binding analysis method for a PET tracer and its radiometabolites: A case study with [11 C]SMW139 to explain the high uptake of radiometabolites in mouse brain. J Pharm Biomed Anal. 2022;219.
25. Brumberg J, Aarnio R, Forsberg A, Marjamäki P, Kerstens V, Moein MM et al. Quantification of the purinergic P2X7 receptor with [11 C]SMW139 improves through correction for brain-penetrating radiometabolites. J Cereb Blood Flow Metab [Internet]. 2023 [cited 2023 Jun 16];43:258–68. https://pubmed.ncbi.nlm.nih.gov/36163685/
26. Sureau FC, Reader AJ, Comtat C, Leroy C, Ribeiro MJ, Buvat I et al. Impact of image-space resolution modeling for studies with the high-resolution research tomograph. J Nucl Med [Internet]. 2008 [cited 2024 Feb 13];49:1000–8. https://pubmed.ncbi.nlm.nih.gov/18511844/
27. Schmidt P, Gaser C, Arsic M, Buck D, Förschler A, Berthele A, et al. An automated tool for detection of FLAIR-hyperintense white-matter lesions in multiple sclerosis. NeuroImage. 2012;59:3774–83.
28. Kanellopoulos JM, Delarasse C. Pleiotropic Roles of P2X7 in the Central Nervous System. Front Cell Neurosci [Internet]. 2019 [cited 2024 Sep 11];13. https://pubmed.ncbi.nlm.nih.gov/31551714/
29. Nutma E, Stephenson JA, Gorter RP, de Bruin J, Boucherie DM, Donat CK et al. A quantitative neuropathological assessment of translocator protein expression in multiple sclerosis. Brain [Internet]. 2019;142:3440–55. https://www.ncbi.nlm.nih.gov/pubmed/31578541

30. Airas L, Rissanen E, Rinne JO. Imaging neuroinflammation in multiple sclerosis using TSPO-PET. Clin Transl Imaging. Springer-Verlag Italia s.r.l.; 2015. pp. 461–73.
31. Airas L, Yong VW. Microglia in multiple sclerosis - pathogenesis and imaging. Curr Opin Neurol [Internet]. 2022 [cited 2023 Jan 24];35:299–306. https://pubmed.ncbi.nlm.nih.gov/35674072/
32. Bodini B, Tonietto M, Airas L, Stankoff B. Positron emission tomography in multiple sclerosis - straight to the target. Nat Rev Neurol [Internet]. 2021; https://www.ncbi.nlm.nih.gov/pubmed/34545219
33. Frischer JM, Weigand SD, Guo Y, Kale N, Parisi JE, Pirko I et al. Clinical and pathological insights into the dynamic nature of the white matter multiple sclerosis plaque. Ann Neurol [Internet]. 2015 [cited 2024 Jan 5];78:710–21. https://pubmed.ncbi.nlm.nih.gov/26239536/
34. Kuhlmann T, Ludwin S, Prat A, Antel J, Brück W, Lassmann H. An updated histological classification system for multiple sclerosis lesions. Acta Neuropathol [Internet]. 2017 [cited 2023 Apr 6];133:13–24. https://pubmed.ncbi.nlm.nih.gov/27988845/
35. Laaksonen S, Saraste M, Nylund M, Hinz R, Snellman A, Rinne J et al. Sex-driven variability in TSPO-expressing microglia in MS patients and healthy individuals. Front Neurol [Internet]. 2024 [cited 2024 Feb 28];15:1352116. https://www.frontiersin.org/articles/https://doi.org/10.3389/fneur.2024.1352116/full
36. Schmidt S, Isaak A, Junker A. Spotlight on P2X7 receptor PET imaging: a bright target or a failing star? Int J Mol Sci. 2023;24(2):1374. https://doi.org/10.3390/ijms24021374.
37. Guneykaya D, Ivanov A, Hernandez DP, Haage V, Wojtas B, Meyer N et al. Transcriptional and Translational Differences of Microglia from Male and Female Brains. Cell Rep [Internet]. 2018 [cited 2024 Jun 5];24:2773–2783.e6. https://pubmed.ncbi.nlm.nih.gov/30184509/
38. Villa A, Gelosa P, Castiglioni L, Cimino M, Rizzi N, Pepe G et al. Sex-Specific Features of Microglia from Adult Mice. Cell Rep [Internet]. 2018 [cited 2024 Jun 5];23:3501–11. https://pubmed.ncbi.nlm.nih.gov/29924994/

Publisher's note